Stable Storage of Helium in Nanoscale Platelets at Semicoherent Interfaces

A. Kashinath, A. Misra, and M. J. Demkowicz

Phys. Rev. Lett. **110**, 086101 — Published 19 February 2013

DOI: 10.1103/PhysRevLett.110.086101

Stable storage of helium in nanoscale platelets at semi-coherent interfaces

A. Kashinath[1*], A. Misra[2], M. J. Demkowicz[1]
[1]Department of Materials Science and Engineering, Massachusetts Institute of Technology, Cambridge, MA 02139
[2]Center for Integrated Nanotechnologies, Los Alamos National Laboratory, Los Alamos, NM 87544
(Received 2 October 2012)

He implanted into metals precipitates into nano-scale bubbles that may later grow into voids, degrading the properties of engineering alloys. Using multiscale modeling, we show that a different class of He precipitates may form at semi-coherent interfaces: nanoscale platelets. These platelets grow by wetting high-energy interface regions, remain stable under irradiation, and reduce He-induced swelling. Stable storage of He at interfaces may impart unprecedented He resistance to future structural materials.

PACS numbers: 68.35.-p, 61.72.J-, 61.82.-d, 61.80.-x

He is a byproduct of nuclear reactions that create α particles (He nuclei) and degrades engineering alloys [1] by accelerating radiation-induced embrittlement [2], swelling [3,4], and surface deterioration [5,6]. Even refractory metals are subject to He damage [7,8]. The insolubility of He is the root cause of its destructiveness: any measurable He concentration in a metal precipitates out into 1-2nm diameter bubbles [9]. Boundaries between crystalline grains are considered especially susceptible to He bubble formation [10,11].

However, at interfaces in certain layered metal composites, no bubbles are observed up to He concentrations of several atomic percent: orders of magnitude higher than the bulk solubility limit [12-14]. In this article, we use multiscale modeling to demonstrate that this surprising absence of bubbles is due to localized wetting of interfaces with nanoscale He platelets that remain stable even under irradiation.

These platelets store He nearly three times more efficiently than spherical bubbles. Because they enable the formation of He platelets, solid-state interfaces—far from being a structural material's weakest links—may reduce He-induced degradation, bringing us a step closer to safe, clean, and inexpensive nuclear energy.

The interfaces of interest here are formed between copper (Cu)—a face centered cubic (fcc) metal—and one of three body centered cubic (bcc) metals: niobium (Nb), molybdenum (Mo), or vanadium (V). We use these semi-coherent interfaces as model systems to explore the interaction between He and the networks of misfit dislocations present in them [15]. For the same interfacial crystallography, misfit dislocation densities increase as: Cu-V > Cu-Mo > Cu-Nb.

Because of its insolubility, He does not permeate into metals from the atmosphere [16]. Instead, it must be implanted at high kinetic energy. Upon coming to rest in a solid, He diffuses until it reaches a trapping site, which — in nanocomposites such as those that motivated this study — is nearly always a semi-coherent interface or, more specifically, a discrete site within it known as a misfit dislocation intersection (MDI), illustrated in Fig. 1. MDIs are an intrinsic part of semi-coherent interfaces [17,18]. Experiments have shown that, on average, ~25 He atoms may be stored at each MDI without forming a bubble [19]—far in excess of the number expected from solubility arguments [20].

Since no experimental method is currently capable of investigating individual He atoms in solids, we turn to atomistic modeling. We choose to model Cu-Nb interfaces because they have been extensively characterized [17,21,22] and a validated embedded atom method (EAM) interatomic potential is available to describe Cu-Nb-He bonding [23,24]. In this potential, interactions of He with other atoms are described using a two-body term that was constructed based on density functional theory (DFT) calculations and therefore does not represent van der Waals interactions [25, 26]. This, however, does not pose a difficulty in our study because such interactions are negligible at interatomic distances characteristic of He

in solid Cu and Nb, namely 2-3Å. The model sizes required to represent non-coherent Cu-Nb interfaces presented here are too large for the study to be carried out using first principles methods alone.

Implantation and diffusion of He is well understood [27,28], so we focus on unit processes of He trapping at MDIs. Once He interactions with MDIs in fcc-bcc interfaces are understood, predictions of He behavior in more complex systems such as metal-oxide interfaces can be made based on the distribution of MDIs in them [19]. As a starting point for our simulations, we use a previously constructed interface model that represents the minimum energy state and experimentally determined crystallography of He-free interfaces in magnetron sputtered Cu-Nb multilayers [17,18]. Formation energies of isolated He defects computed using this model are lower at the Cu-Nb interface than in fcc Cu or bcc Nb. Within the interface, they are lowest at MDIs in the Cu terminal plane (see supplement 1).

At the implantation rate used in experiments [12,22], the average time between successive He atom arrivals near a MDI is ~10 minutes. At room temperature, this interval is sufficient not only for every implanted atom to reach an MDI before the next one arrives, but also for the free volume at the MDI to equilibrate through interfacial vacancy diffusion [29,30]. Therefore, to simulate He trapping we adopt an iterative approach—detailed in supplement 2—for adding He atoms to the interface while allowing the number of vacancies in it to adjust freely.

We find that successively added He atoms aggregate into clusters, illustrated in Fig. 2. As expected, these clusters form at MDIs. Their He-to-vacancy ratio is slightly smaller than unity and decreases with increasing cluster size. Because vacancy formation energies in Nb are about twice as high as in Cu [18], He clusters grow exclusively into the Cu side of the interface. Furthermore, there is always a thermodynamic driving force for separate He clusters to join into one cluster: the sum of energies of two clusters containing n_1 and n_2 He atoms is always higher than the energy of a single cluster containing (n_1+n_2) atoms. The longevity of separate

clusters at multiple MDIs must therefore be attributed to low rates of coarsening and coalescence.

Most importantly, our study revealed that there are two distinct modes of He cluster growth at Cu-Nb interfaces. As shown in Fig. 2 (a)-(c), up to ~20 He atoms, the clusters are two atomic layers thick and grow as flat platelets by increasing the interface area they occupy. When their size increases beyond 20 He atoms, however, the clusters grow by increasing their thickness one layer at a time while maintaining a constant area along the interface, as shown in Fig. 2 (c)-(e).

This change in growth mode is due to interface wetting. Three surface energies are relevant for the shape and location of the clusters in Fig. 2: the Cu-He and Nb-He surface energies γ_{CuHe} and γ_{NbHe} and the interface energy γ_{CuNb}. They define an excess interface wetting energy: $W = \gamma_{CuNb} + \gamma_{CuHe} - \gamma_{NbHe}$ [31]. When W<0, a He cluster has lowest energy when it is entirely within the Cu and does not touch the interface. When W>0, its energy is lowest when it wets the interface—much like a water drop on a glass pane—at a contact angle that depends on the surface energies. Using molecular statics, we calculated that $\gamma_{CuHe} = 1.93 J/m^2$, $\gamma_{NbHe} = 2.40 J/m^2$, and the *average* Cu-Nb interface energy $\overline{\gamma}_{CuNb} = 0.54\ J/m^2$. The average wetting energy is therefore marginally positive, suggesting that He clusters of any size should wet the interface, albeit with high contact angle.

Over distances comparable to the dimensions of the He clusters in Fig. 2, however, γ_{CuNb} is not uniform. We determined its spatial variation by cutting out of the Cu layer a cylinder whose base lies in a He-free Cu-Nb interface and has a 5Å radius. A reference cylinder of the same dimensions is cut from an identically oriented block of fcc Cu. The energy difference between the two cylinders is used to compute the local value of γ_{CuNb} on a patch of radius 5Å. Scanning the location of the first cylinder over the interface, γ_{CuNb} is found to vary with position as shown in Fig. 3: ~$1nm^2$-

sizes patches with γ_{CuNb} as high as 0.8J/m^2 are separated by regions with γ_{CuNb} as low as 0.4J/m^2.

The spatial heterogeneity of γ_{CuNb} explains the change in growth mode of He clusters at Cu-Nb interfaces. The high-energy patches coincide with MDIs and have large positive W values. Small He clusters therefore grow by wetting these regions at low contact angles. Once a cluster has grown larger than ~1nm^2, however, W becomes negative in the area between MDIs and no further wetting is possible. Subsequent growth of the cluster proceeds into the Cu layer while its area of contact with the interface remains unchanged.

A remarkable consequence of how the clusters grow is that there is a rapid decrease in $\frac{\partial E_s}{\partial V}$—the derivative of the cluster's surface energy E_s with respect to its volume V—when the growth mode changes, illustrated in Fig. 4. This has important consequences for the stability of He clusters under irradiation. For a fixed number of He atoms, $\dot{V}$—the rate of change of V —is determined by net fluxes of point defects into a cluster: a net flux of vacancies increases V while a net flux of interstitials decreases it. Each net flux, in turn, is a difference between two contributions: a flux of radiation-induced defects into the cluster minus the outward flux of defects created at the cluster surface by thermal emission. Due to the high formation energy of interstitials, their thermal emission may be neglected. On the other hand, the concentration of thermally emitted vacancies at the cluster surface [32,33], $c_v^{surface} = c_v^{eq} e^{-\left(P_{He} - \frac{\partial E_s}{\partial V}\right)\frac{\Omega}{k_B T}}$, generally cannot be neglected and is highly sensitive to $\frac{\partial E_s}{\partial V}$. c_v^{eq} is the equilibrium vacancy concentration in fcc Cu, P_{He} is He pressure in the cluster, and Ω is atomic volume.

Net defect fluxes may be used to calculate $\dot{V}$ as a function of V. We computed these fluxes for experimental irradiation conditions [12,22] from a system of continuum

reaction-diffusion equations using the finite element method (FEM), as described in supplement 3. We described the shape of clusters at different stages of growth by a simple spherical cap model, illustrated in the inset of Fig. 4. This model was parameterized using only the location-dependent γ_{CuNb} values in Fig. 3, but represents $\frac{\partial E_s}{\partial V}$ remarkably well: the solid line in Fig. 4 was computed analytically from the model with no further fitting.

Fig. 5 compares $\dot{V}(V)$ for an 18-atom He cluster at a Cu-Nb interface and in perfect fcc Cu. The latter has two equilibrium values of V, where $\dot{V} = 0$: a stable equilibrium point at low volume (perturbations in V create $\dot{V}$ values that restore equilibrium) and an unstable one at high volume (perturbations in V grow). This corresponds to the well-known distinction between stable He-filled "bubbles" and unstable "voids" that grow indefinitely by vacancy capture [32,33].

By contrast, $\dot{V}(V)$ for the interfacial He cluster shows *three* equilibrium points: *two* stable ones at low volume and an unstable one at high volume. The latter is the critical volume required to form an unstable interface void. The stable equilibrium point of higher volume is an approximately spherical bubble, analogous to bubbles in single crystals. The lower volume equilibrium point, however, is a new type of stable He cluster: an interfacial He platelet, such as those shown in Fig 2 (a)-(c). These platelets owe their remarkable stability under irradiation to their relatively high $\frac{\partial E_s}{\partial V}$ value at low volume, shown in Fig. 4, and lose stability as $\frac{\partial E_s}{\partial V}$ drops when the He cluster growth mode changes. The He clusters in Fig. 2 (d)-(e) are beyond the range of stable volumes computed using our FEM models and would therefore grow rapidly by vacancy capture into approximately spherical He filled bubbles.

Nanoscale He bubbles at interfaces are typically revealed via through-focus imaging in transmission electron microscopy (TEM) [9]. He platelets [Fig. 2 (a)-(c)] may be

too small to resolve using this technique. Our finding, however, does explain why a critical He concentration is required to observe bubbles using TEM at interfaces in magnetron sputtered multilayers [12-14]: as the number of He atoms in a platelet increases, the range of volumes at which it is stable shrinks and eventually vanishes. Our FEM calculations predict that, under experimental conditions, this occurs when there are 21 atoms in the cluster, in good agreement with previous deductions of 25 atoms per MDI [19]. Once the platelet shape becomes unstable under irradiation, the cluster volume grows until it reaches the next stable equilibrium point, shown in Fig. 5, resulting in a 150% volume increase and an approximately spherical bubble that can be resolved by TEM [9].

The existence of stable, interface-wetting He platelets has far-reaching implications for the design of He-resistant materials for future fusion and advanced fission reactors. For example, we calculate that, in the experiments that motivated this work, the volume of such platelets is nearly three times smaller than that of bubbles in fcc Cu with the same number of He atoms. Platelets therefore store He more efficiently than spherical bubbles and lead to less He-induced swelling prior to void formation.

Stable nanoscale He platelets are not restricted to fcc-bcc model interfaces. On the contrary, they may be ubiquitous: all that is required for their formation is an interface whose location-dependent energy gives rise to wetting by He on isolated interface patches. In fact, by controlling interface structure, the size and distribution of interfacial wetting regions may be *designed*: e.g. MDIs may be arranged to link up into continuous pathways for controlled He outgassing. To ensure that implanted He reaches such designer interfaces before forming immobile clusters or bubbles within crystalline grains, materials with a large interface area per unit volume are required. The nanolaminates that motivated this study are one example of such materials. Nanoferritic alloys (NFAs) [34], which contain a high density of nanoscale oxide precipitates, are another. Platelet formation may occur during the initial stages of He trapping at interfaces between these precipitates and the surrounding

Fe matrix. This may explain the high initial resistance of NFAs to He-induced damage and suggests that it may be further enhanced through improved control of the matrix-precipitate interfaces.

We thank A. Caro, G. R. Odette, T. Lee, K. Kolluri, and R. E. Baumer for useful discussions. This work was supported by the Center for Materials in Irradiation and Mechanical Extremes (CMIME), an Energy Frontier Research Center funded by the U. S. Department of Energy, Office of Science, Office of Basic Energy Sciences under award number 2008LANL1026

Figures:

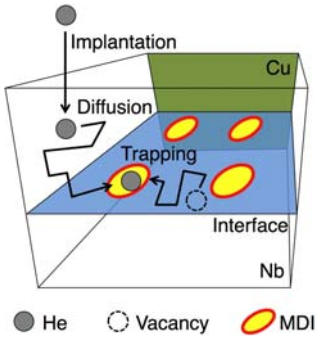

FIG. 1 (color online). Stages of He introduction into MDIs at Cu-Nb interfaces.

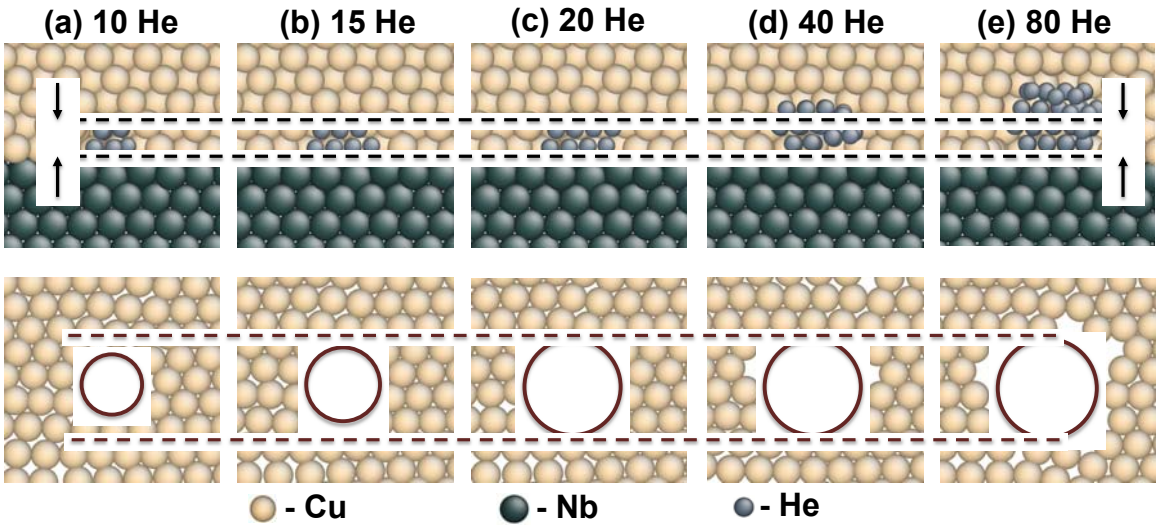

FIG. 2 (color online). Two growth modes of He-vacancy clusters at a MDI: parallel to the interface (a)-(c); normal to the interface (c)-(e). Top row: edge-on view of Cu-Nb interface. Bottom row: in-plane view of interface Cu terminal plane. (Author note: Figure spans 2 columns)

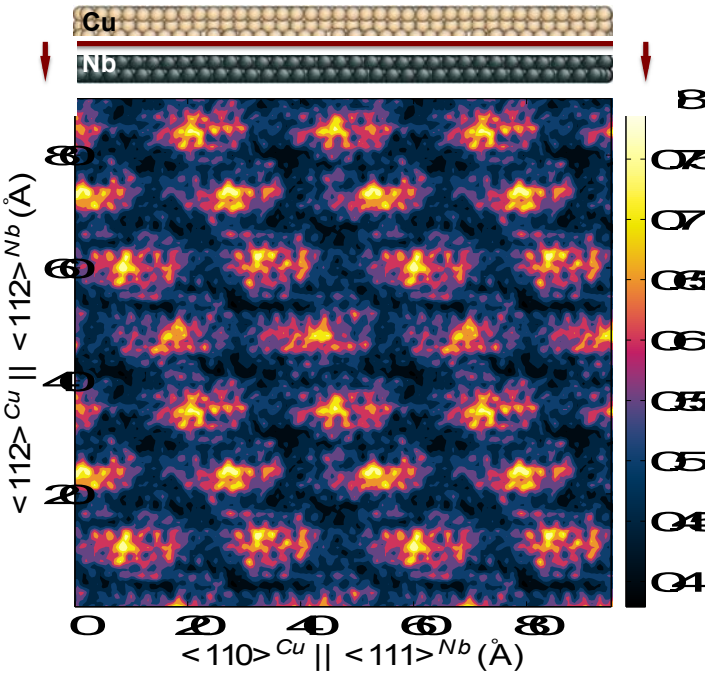

FIG. 3 (color online). Location dependence of γ_{CuNb} (J/m^2), looking normal to the interface plane. Patches of highest energy coincide with MDIs.

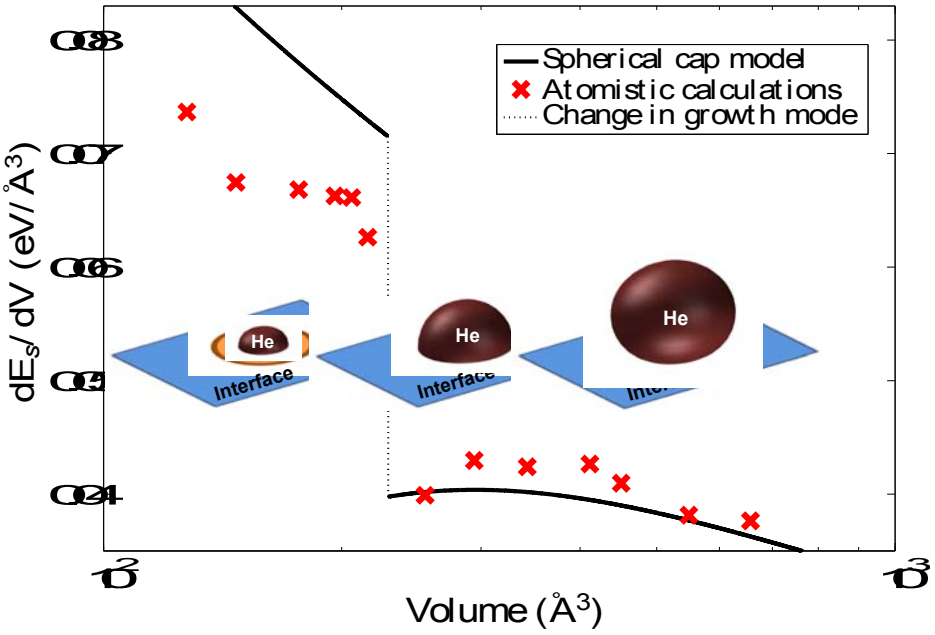

FIG. 4 (color online). The dependence of $\frac{\partial E_s}{\partial V}$ on V. The insets illustrate a spherical cap model of He cluster growth.

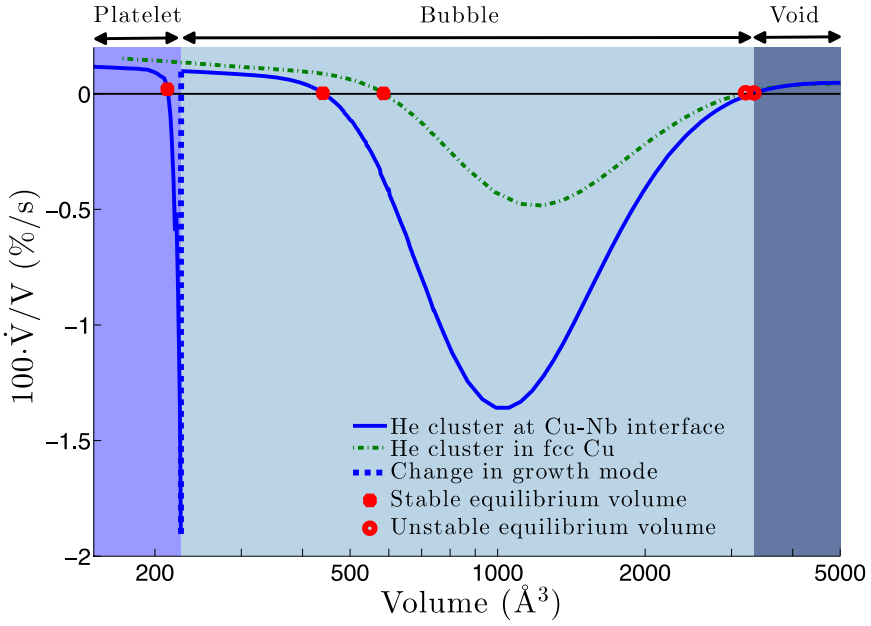

FIG. 5 (color online). $\dot{V}(V)$ for an 18-atom He cluster at a Cu-Nb interface and in perfect fcc Cu.

* - Corresponding Author

abishekk@mit.edu

References:

[1] H. Ullmaier, *Nucl. Fusion* **24**, 1039 (1984).
[2] H. Schroeder, W. Kesternich, and H. Ullmaier, *Nucl. Eng. Des./Fusion* **2**, 65 (1985).
[3] K. Farrell, *Radiat. Eff. Defects Solids* **53**, 175 (1980).
[4] S. J. Zinkle, W. G. Wolfer, G. L. Kulcinski, and L. E. Seitzman, *Philos. Mag. A* **55**, 127 (1987).
[5] R. E. Galindo, A. van Veen, J. H. Evans, H. Schut, and J. T. M. de Hosson, *Nucl. Instrum. Methods Phys. Res., Sect. B* **217**, 262 (2004).
[6] J. H. Evans, R. E. Galindo, and A. van Veen, *Nucl. Instrum. Methods Phys. Res., Sect. B* **217**, 276 (2004).
[7] S. Kajita, W. Sakaguchi, N. Ohno, N. Yoshida, and T. Saeki, *Nucl. Fusion* **49**, 095005 (2009).
[8] S. Sharafat, A. Takahashi, Q. Hu, and N. M. A. Ghoniem, *J. Nucl. Mater.* **386-88**, 900 (2009).
[9] D. Bhattacharyya *et al.* , *Microsc. Microanal.* **18**, 152 (2012).
[10] P. L. Lane, and P. J. Goodhew, *Philos. Mag. A* **48**, 965 (1983).
[11] B. N. Singh, T. Leffers, W. V. Green, and M. Victoria, *J. Nucl. Mater.* **125**, 287 (1984).
[12] M. J. Demkowicz *et al.* , *Appl. Phys. Lett.* **97**, 161903 (2010).
[13] E. G. Fu, A. Misra, H. Wang, L. Shao, and X. Zhang, *J. Nucl. Mater.* **407**, 178 (2010).
[14] N. Li *et al.* , *Philos. Mag. Lett.* **91**, 19 (2010).
[15] A. P. Sutton, and R. W. Balluffi, *Interfaces in Crystalline Materials* (Oxford Univ. Press, Oxford, 1995).
[16] J. Laakmann, P. Jung, and W. Uelhoff, *Acta Metall.* **35**, 2063 (1987).
[17] M. J. Demkowicz, R. G. Hoagland, and J. P. Hirth, *Phys. Rev. Lett.* **100**, 136102 (2008).
[18] M. J. Demkowicz, J. Wang, and R. G. Hoagland, *Dislocations in Solids*, edited by J. P. Hirth (Elsevier, 2008), Vol. 14, Ch.83, 141
[19] M. J. Demkowicz, A. Misra, and A. Caro, *Curr. Opin. Solid State Mat. Sci.* **16**, 101 (2012).
[20] P. Erhart, *J. Appl. Phys.* **111**, 113502 (2012).
[21] J. Wang, and A. Misra, *Curr. Opin. Solid State Mat. Sci.* **15**, 20 (2011).
[22] A. Misra, M. J. Demkowicz, X. Zhang, and R. G. Hoagland, *JOM* **59**, 62 (2007).
[23] M. J. Demkowicz, and R. G. Hoagland, *Int. J. Appl. Mech.* **1**, 421 (2009).
[24] A. Kashinath, and M. J. Demkowicz, *Model. Simul. Mater. Sci. Eng.* **19**, 035007 (2011).
[25] N. Jean, M. I. Trioni, G. P. Brivio, and V. Bortolani, *Phys. Rev. Lett.* **92**, 013201 (2004).
[26] J. L. F. Da Silva, C. Stampfl, and M. Scheffler, *Phys. Rev. Lett.* **90**, 066104 (2003).

[27] K. O. E. Henriksson, K. Nordlund, J. Keinonen, D. Sundholm, and M. Patzschke, *Phys. Scr.* **T108**, 95 (2004).
[28] F. Gao, H. L. Heinisch, and R. J. Kurtz, *J. Nucl. Mater.* **367**, 446 (2007).
[29] K. Kolluri, and M. J. Demkowicz, *Phys. Rev. B* **82**, 193404 (2010).
[30] K. Kolluri, and M. J. Demkowicz, *Phys. Rev. B* **85**, 205416 (2012).
[31] P. -G. de Gennes, F. Brochard-Wyart, and D. Quéré, *Capillarity and Wetting Phenomena: Drops, Bubbles, Pearls, Waves* (Springer, 2004).
[32] L. K. Mansur, and W. A. Coghlan, *J. Nucl. Mater.* **119**, 1 (1983).
[33] R. E. Stoller, and G. R. Odette, *J. Nucl. Mater.* **131**, 118 (1985).
[34] G. R. Odette, and D. T. Hoelzer, *JOM* **62**, 84 (2010).